Palaeogeography, Palaeoclimatology, Palaeoecology 687 (2026) 113590

Contents lists available at ScienceDirect

Palaeogeography, Palaeoclimatology, Palaeoecology

journal homepage: www.elsevier.com/locate/palaeo

Abyssal record of the Middle Eocene Climatic Optimum in the Tasman Sea: Insights from benthic foraminiferal and clay mineral assemblages

Irene Peñalver-Clavel [a,*], Elisa Laita [b], Edoardo Dallanave [c], Rupert Sutherland [d], Gerald R. Dickens [e], Thomas Westerhold [f], Blanca Bauluz [a], Laia Alegret [a]

[a] Departamento de Ciencias de la Tierra & IUCA, Universidad de Zaragoza, 50009 Zaragoza, Spain
[b] Departamento de Geología & Centro de Estudios Avanzados en Ciencias de la Tierra, Energía y Medio Ambiente (CEACTEMA), Universidad de Jaén, 23071 Jaén, Spain
[c] Dipartimento di Scienze della Terra "Ardito Desio", Università degli Studi di Milano, 20133 Milano, Italy
[d] SGEES, Victoria University of Wellington, P.O. Box 600, Wellington 6140, New Zealand
[e] Department of Geology, School of Natural Sciences, Trinity College Dublin, 2 Dublin, Ireland
[f] Center for Marine Environmental Sciences (MARUM), University of Bremen, 28359 Bremen, Germany

ARTICLE INFO

Keywords:
Eocene
SW Pacific
Warming
Benthic foraminifera
Abyssal
Mineralogy
Tasman Sea

ABSTRACT

The Middle Eocene Climatic Optimum (MECO), a ~500 kyr global warm interval at ~40 Ma, interrupted the gradual cooling trend of the mid-late Eocene. Unlike Eocene hyperthermal events with rapid onsets and slow recoveries, the MECO began gradually, ended swiftly, and lacked a global negative carbon isotope excursion, raising questions about warming-carbon cycling links. Here we report for the first time the response of benthic foraminifera, which are excellent palaeoenvironmental proxies, across the MECO at abyssal depths, integrating our results with a mineralogical analysis of the sediment.

International Ocean Discovery Program Site U1511 (Tasman Abyssal Plain, SW Pacific) was deposited below the carbonate compensation depth during the Eocene, and calcareous microfossils are absent. Agglutinated benthic foraminifera indicate a gradual onset of the environmental perturbations associated with the MECO, followed by rapid recovery. Changes in their assemblages, including the temporary disappearance of Lazarus taxa, the decreased abundance of suspension feeders and dominance of opportunistic detritivores, indicate weaker bottom-water currents during MECO and increased stratification of the water column. Mineralogical changes reinforce this interpretation, with increased smectite content indicating warm, humid conditions in the source-area, and possibly a change in the deep-water source. The reappearance of Lazarus taxa after the MECO indicates rapid recovery of deep-sea environmental conditions.

The comparison of Site U1511 with available studies from other regions reveals the complex and regionally diverse nature of benthic foraminiferal response to the MECO, emphasizing the critical role of ocean circulation and palaeogeography during Eocene warm intervals.

1. Introduction

The long-term warming and cooling trends of the Eocene were punctuated by short-lived (<100 kyr) transient global warming events called hyperthermals. These events were typically characterised by paired negative oxygen and carbon isotope excursions in marine carbonate precipitated in all ocean water masses (e.g., Zachos et al., 2008; Westerhold et al., 2017). The Middle Eocene Climatic Optimum (MECO), a warm interval centered around 40.2 Ma, interrupted the long-term cooling trend of the Eocene (e.g., Bohaty et al., 2009; Westerhold et al., 2020). Compared to the hyperthermal events, it had a prolonged duration of ~300 kyr (Rivero-Cuesta et al., 2019) to ~500 kyr (Westerhold and Röhl, 2013) or ~650 kyr (e.g., Bohaty et al., 2009; Edgar et al., 2010), and a range of $\delta^{13}C$ signals in marine carbonates (e.g., Moebius et al., 2015; Gandolfi et al., 2024). Global $\delta^{18}O$ values and organic biomarker proxies for palaeotemperature (UK_{37} and TEX_{86}) indicate that a gradual warming of 3–6 °C in surface and bottom waters started around 40.6 Ma, peaked around 40.0 Ma, and rapidly returned to near pre-MECO temperatures (e.g., Bohaty and Zachos, 2003; Bohaty et al., 2009; Edgar et al., 2010; Bijl et al., 2010). This was associated with increased atmospheric pCO_2 concentrations (Bijl et al., 2010; Henehan et al., 2020), a reduction in surface ocean pH (Henehan et al.,

* Corresponding author.
E-mail address: irenepc@unizar.es (I. Peñalver-Clavel).

https://doi.org/10.1016/j.palaeo.2026.113590
Received 11 April 2025; Received in revised form 9 December 2025; Accepted 21 January 2026
Available online 27 January 2026

2020) and a decline in ocean carbonate accumulation (e.g., Lyle et al., 2005; Pälike et al., 2012). The absence of a global negative $\delta^{13}C$ excursion during the MECO suggests the accumulation of carbon from volcanic (rather than organic) sources in the exogenic carbon pool, i.e., the carbon in the atmosphere, in the oceans, and in the biosphere (e.g., Bohaty et al., 2009; Bijl et al., 2010; Van der Ploeg et al., 2018; Steinthorsdottir et al., 2019; Henehan et al., 2020).

The MECO affected biota in both the deep (e.g., Bohaty and Zachos, 2003; Bohaty et al., 2009; Moebius et al., 2015; Boscolo-Galazzo et al., 2015; Rivero-Cuesta et al., 2019) and surface oceans (Boscolo-Galazzo et al., 2014; Cramwinckel et al., 2018, 2019, 2020). Shifts in planktic and benthic assemblages documented by these studies across the MECO have been linked to global warming and changes in oceanic productivity and oxygenation, at a time of a strengthened hydrological cycle and enhanced runoff (e.g., Moebius et al., 2014, 2015; Gandolfi et al., 2024). At deeper sites (>1000 m) in the Southern Ocean (Fig. 1), changes in relative abundance of benthic foraminiferal species suggest oxygen-depleted bottom waters during the peak warming phase, which is supported by other geochemical indicators (e.g., cerium content on fish teeth) (Moebius et al., 2014). Subtler changes have been reported from shallower sites in northwestern Italy, with planktic and benthic foraminifera and calcareous nannofossils all showing biological adaptations to warmer, nutrient-enriched conditions (e.g., Gandolfi et al., 2024). The few studies carried out in the Pacific Ocean focus on particular settings such as the Tasmanian Gateway (Fig. 1), which makes it challenging to extrapolate their results to the rest of the Pacific Ocean (e.g., Cramwinckel et al., 2020). So far, no records exist of abyssal (>2000 m) benthos communities, as previous studies have focussed on carbonate-rich records where traditional palaeoceanographic records can be generated.

The Tasman Sea, between Australia and New Zealand (Fig. 2), is an interesting region to investigate palaeoceanographic and palaeoclimatic changes during the Eocene, including across various warming events (Alegret et al., 2021a; Peñalver-Clavel et al., 2024). Geochemical data and models indicate that the Southern Ocean, and particularly the southwest Pacific, was the primary area of intermediate and deep-water formation during the early Paleogene (Sijp et al., 2014; Huck et al., 2017; Baatsen et al., 2020; Zhang et al., 2022; Peñalver-Clavel et al., 2025), with water masses flowing through the Tasman Sea. Palynological and organic geochemical records from the central Tasmanian Gateway (Ocean Drilling Program Site 1170), the Otway Basin (southeastern Australia), and the Hampden Beach section (New Zealand) point to warm temperate rainforests on the nearby landmasses, and elevated sea-surface temperatures in the Tasmanian Gateway, suggesting a surface ocean circulation shift and a regional southeast Australian transgression during the MECO (Cramwinckel et al., 2020).

The MECO event has been primarily studied in pelagic carbonate-rich records, yielding well-preserved carbonate for stable isotopes measurements (e.g., Bohaty et al., 2009; Edgar et al., 2010). However, due to increased ocean acidity from the MECO warming, the carbonate compensation depth (CCD) shoaled (Henehan et al., 2020), making it challenging to find carbonate-based evidence in the deepest ocean.

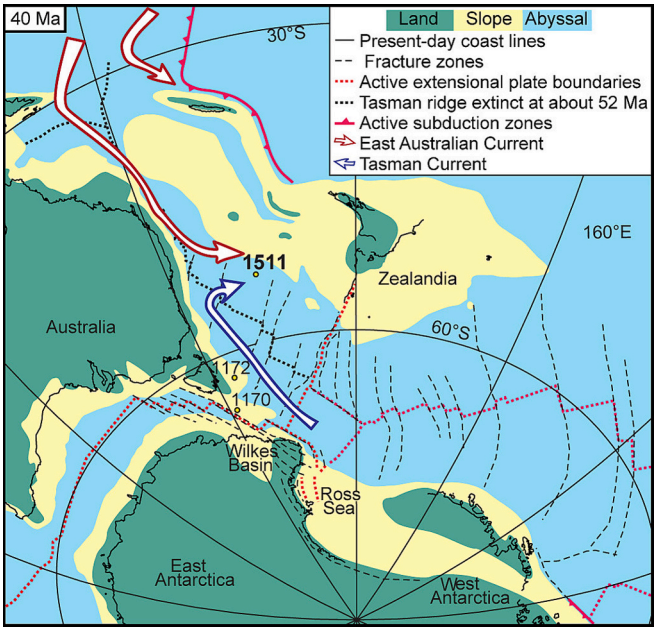

Fig. 2. Palaeogeography of study area at 40 Ma, reconstructed with GPlates (https://www.gplates.org/), with surface currents and sites where the MECO has been studied in the Tasman Sea: ODP Sites 1170 and 1172 (Cramwinckel et al., 2020), IODP Site U1511 (this study).

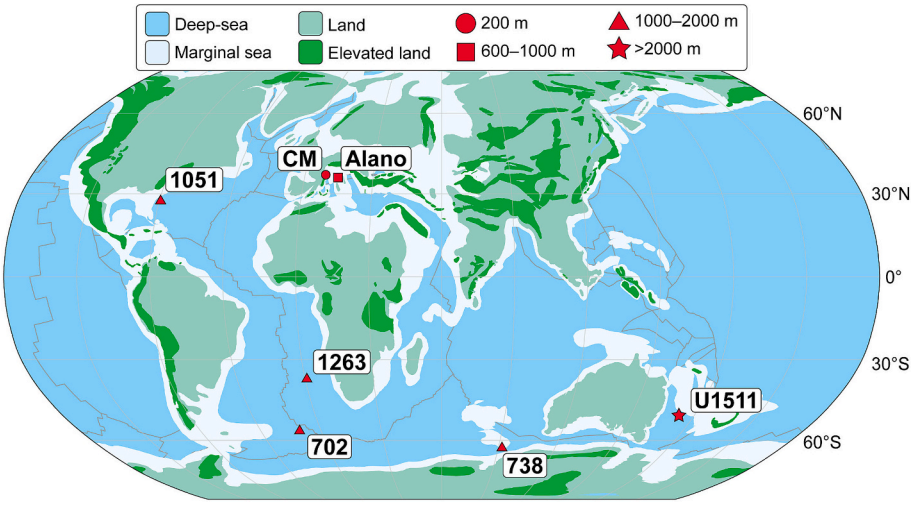

Fig. 1. Paleogeographic maps at 40 Ma, and sites with studies of benthic foraminifera across the MECO. The palaeogeographic positions of all tectonic plates units was calculated by anchoring the relative plate motion model of Müller et al. (2016) to the Earth's spin axis, using seven paleomagnetic poles from the literature (Supplementary Information, Table S1), GPlates (Müller et al., 2018) and PmagDiR (Dallanave, 2024). The main paleogeographic features are from Cao et al. (2017). CM, Capo Mortola. Sites: Alano (Boscolo-Galazzo et al., 2013) and Capo Mortola (CM; Gandolfi et al., 2024) sections in the western Tethys Ocean, North Atlantic ODP Site 1051 (Moebius et al., 2015), South Atlantic ODP Sites 1263 (Boscolo-Galazzo et al., 2015) and 702 (Rivero-Cuesta et al., 2019), ODP Site 738 from the Indian Southern Ocean (Moebius et al., 2014), and Pacific Ocean IODP Site U1511 (this study).

Well away from the coast, the MECO has been identified at IODP Site U1511 in the Tasman Abyssal Plain, providing a unique record of environmental change below the CCD. Increased water-column stratification, and decreased surface and export productivity have been inferred across the MECO at this site based on magnetic, mineralogical and geochemical analyses (Sutherland et al., 2019; Cornaggia et al., 2020), but the response of deep-sea biota has not been documented so far.

Benthic foraminifera are the most common group of meiofaunal unicellular organisms in the dark, cold and nutrient-deprived deep-sea, and they are excellent tools to reconstruct the environmental conditions and deep-water masses (Alegret et al., 2021b). Their response to MECO warming has been documented from locations in the palaeo-Tethys seaway (e.g., Boscolo-Galazzo et al., 2013; Gandolfi et al., 2024), the Atlantic Ocean (Boscolo-Galazzo et al., 2014; Moebius et al., 2015; Rivero-Cuesta et al., 2019), and in the Southern Ocean (Moebius et al., 2014). Herein, the first record of deep-sea benthic foraminifera across the MECO in an abyssal environment below the CCD is presented. Deep-water agglutinated foraminifera (DWAF) are often the only benthic microfossils preserved in the deep-water sediments deposited beneath the CCD, and assemblages from abyssal plains thrive in environments with low sedimentation and low organic flux, representing the most oligotrophic end of the spectrum (Kaminski and Gradstein, 2005). Paleocene and early Eocene DWAF from Site U1511 were documented in the scientific results of IODP Expedition 371 (Sutherland et al., 2019), and by Kaminski et al. (2021, 2024a, 2024b). The lack of benthic foraminiferal records across the MECO at abyssal (>2000 m) depths below the CCD highlights the unique and significant contribution of this study to the understanding of deep-sea environments during warming events. The analysis of benthic foraminiferal assemblages from Site U1511, along with whole rock and clay fraction mineralogical studies, document the palaeoenvironmental consequences of prolonged MECO warming and global carbon cycle disturbance.

2. The MECO at Site U1511 (Tasman Sea)

2.1. Location and geological setting

IODP Expedition 371 drilled Site U1511 (37.5611°S, 160.3156°E) on the Tasman Abyssal Plain in the southwest Pacific Ocean, ~945 km east of Australia and ~990 km northwest of New Zealand (Fig. 2) (Sutherland et al., 2019). Site U1511 currently lies at 4847 m water depth, below the present-day CCD and the southern extent of the East Australian Current, a component of the South Pacific Gyre (Huber et al., 2004; Cramwinckel et al., 2020) (Fig. 2).

During the Eocene, the ocean circulation and climate were significantly influenced by tectonic shifts in the southwest Pacific, which altered oceanic pathways and heat transport (e.g., Baatsen et al., 2020). The Tasmanian Gateway and Drake Passage began to open and deepen (e.g., Bijl et al., 2013), while the Australian continent transitioned from a northwesterly to a northerly movement (e.g., Cande and Stock, 2004). Subduction initiated in Zealandia, impacting vertical motion in areas such as the Lord Howe Rise (Sutherland et al., 2020), alongside subsidence along the outer continental shelves (e.g., Totterdell et al., 2000).

Sediments from Site U1511 were deposited at abyssal depths during the middle Eocene (Sutherland et al., 2019). By this time, models of ocean-atmosphere dynamics suggest that an early version of the South Pacific Gyre drove global ocean heat transport, but it was less intense than in present times, due to the partial closure of the seaway between Australia and Antarctica (Huber et al., 2004). The intensification of the gyre occurred as the Southern Ocean expanded and Antarctica experienced cooling (Kennett, 1977). The northern edge of the Tasman Abyssal Plain was influenced by a southeast-flowing precursor to the Eastern Australian Current (EAC), while its southern edge was bounded by the northward-flowing Tasman Current (TC) (Huber et al., 2004; Cramwinckel et al., 2020) (Fig. 2). The EAC, moving southward along the eastern coast of Australia, was characterised by warm, saline, and nutrient-poor waters at surface and intermediate depths. Conversely, the TC was a cooler, wind-driven current traveling northward along the same coastline (Huber et al., 2004; Bijl et al., 2011).

2.2. Identification of the MECO below the CCD

Originally defined by a distinct negative shift in $\delta^{18}O$ values (~1.0‰) in marine carbonate (Bohaty and Zachos, 2003), the MECO is typically marked by negative oxygen isotope excursions in marine bulk sediment and benthic foraminifera (e.g., Bohaty and Zachos, 2003; Rivero-Cuesta et al., 2019). The lack of carbonate in the study record at Site U1511 prevented classical identification of the MECO; however, the peak MECO closely aligns with the base of polarity Chron C18n.2n, which provides a firm age constraint (Bohaty et al., 2009; Cornaggia et al., 2020).

The MECO was identified at Site U1511 during IODP Expedition 371, in the middle of Core 371-U1511B-16R, based on magnetic inclination and the top of the radiolarian species *Artobotrys biaurita*, which usually occurs in Zone zRP14 (Sutherland et al., 2017, 2019). Despite being collected via rotary coring methods, drilling disturbance did not affect the record of the MECO across a 3.5 m interval (between 264 and 267.5 m CSF-A), which coincides with significant changes in physical properties (darker colour, elevated magnetic susceptibility and higher natural gamma radiation) (Sutherland et al., 2019). Radiolarians are common to abundant and well preserved. The lack of calcareous fossils (planktic foraminifera, calcareous nannofossils and calcareous benthic foraminifera) in Pliocene to early Eocene and upper Paleocene samples suggests that Site U1511 was located below the CCD for much of the Cenozoic, at lower bathyal-abyssal depths, with an interval of the Paleocene (towards the base of Hole U1511B, 528.06–560.79 m) containing a few specimens of calcareous benthic foraminifers, rare planktic foraminifers, and a few poorly preserved calcareous nannofossils along with agglutinated benthic foraminifers, which may indicate when sediments accumulated above the CCD but below the lysocline (Sutherland et al., 2019). X-ray diffraction (XRD) analyses of Eocene samples conducted during IODP Expedition 371 indicated a mineralogy with variable proportions of quartz (as detrital silt), illite, montmorillonite (smectite) and kaolinite (Sutherland et al., 2019).

3. Material and methods

3.1. Study interval and age model

For this study, the shipboard age model from Site U1511 (Sutherland et al., 2019) was updated by reassigning ages of magnetostratigraphic and radiolarian events according to the Geological Time Scale 2020 (GTS2020; Gradstein et al., 2020) (Suppl. Mat., Table S2). The refined age model, which includes new magnetostratigraphy data (Dallanave and Chang, 2020), allows a variable-resolution sampling strategy for benthic foraminiferal studies. Samples were collected at a coarse resolution of 30–90 cm below and above the event to observe general trends, and at a higher resolution (19–20 cm) across the MECO and proximal depths for a more detailed palaeoclimatic and palaeoenvironmental reconstruction.

The study interval ranges from Hole 1511B-16R-1, 24–26 cm, to 17R-5, 85–87 cm (259.75–275.96 m CSF-A). It consists of greenish grey to yellowish brown diatomite and claystone with varying amounts of other bio-siliceous components (Sutherland et al., 2019).

3.2. Benthic foraminifera

A total of 38 samples (Suppl. Mat., Table S3) were analysed for the study of benthic foraminiferal assemblages. Sediment samples (20 cc) were dried in an oven at 40 °C, weighed, and soaked in sodium hexametaphosphate ($Na_6(PO_3)_6$) for four hours. Disaggregated samples

were then washed over a >63 μm size fraction sieve, and the remaining residue was oven-dried and weighed. Among biogenic components, benthic foraminifera are rare compared to the total sediment particles in the >63 μm studied fraction, which mainly consist of radiolarians, sponge spicules, and fish debris (Sutherland et al., 2019). The total number of benthic foraminifera per sample did not reach the typical threshold of 250–300 specimens per sample that are commonly used in quantitative analyses. Therefore, a semi-quantitative study of the assemblages was carried out due to the limited number of individuals. The whole residue was analysed with an Olympus-SDF PLAPO 1XPF reflected-light microscope, and all benthic foraminifera specimens were picked and placed in micropalaeontological slides for a permanent record. The slides are housed in the IODP 371 collection of the Benthic Foraminifera and Global Change Lab of the Department of Earth Sciences at Zaragoza University, Spain.

Taxonomic classification follows species and genus concepts presented in previous works (Alegret and Thomas, 2001; Arreguín-Rodríguez et al., 2013; Kaminski and Gradstein, 2005). To determine the abundance of each species per gram of sediment, the raw data matrix with the benthic foraminiferal counts (Suppl. Mat., Table S3) and the weight of bulk rock sediment and of the picked residue were used. The limited number of individuals found in the available residue precludes the calculation of relative abundances. However, the number of individuals (in total, and number of individuals of each taxon), plus the estimated number of individuals per gram of sediment, were calculated (Fig. 3). The Fisher- α diversity was calculated using a numerical method (http://groundvegetationdb-web.com/ground_veg/home/diversity_index). Specimens of the most representative taxa were gold coated and photographed using the Scanning Electron Micrograph imaging facilities (JEOL JSM 6360-LV) of the University of Zaragoza (Spain) (Fig. 4).

3.3. Other components of the sediment

After picking the scarce benthic foraminifera, a qualitative analysis of remaining components of the sediment was carried out in the washed >63 μm size fraction. The washed residue was examined on a sampling tray, and the proportions of radiolarians, terrigenous material and sponge spicules were recorded based on their observed percentage in each sample. Following Sutherland et al. (2019), the components were classified according to their relative abundance: barren (B, 0%), rare (R, <10%), common (C, 10–50%), abundant (A, 50–80%), or dominant (D, >80%) (Fig. 5A; Suppl. Mat., Table S4). Additionally, photographs of the samples were taken to illustrate compositional differences throughout the study section (Fig. 5B, C).

3.4. X-ray diffraction

A total of 18 samples were selected for mineralogical analyses of whole, bulk rock sediment and the <2 μm fraction (Suppl. Mat., Table S5). The <2 μm fraction was extracted by centrifugation of bulk sediment. From residues, both air-dried and ethylene glycol-treated oriented aggregates were prepared to obtain enhanced basal reflections of the clay minerals. The purpose of analysing <2 μm fraction with greater detail was to observe clay mineral assemblage variations through the studied section.

X-ray diffraction (XRD) patterns were obtained using the Philips 1710 diffractometer at the University of Zaragoza with a voltage of 40

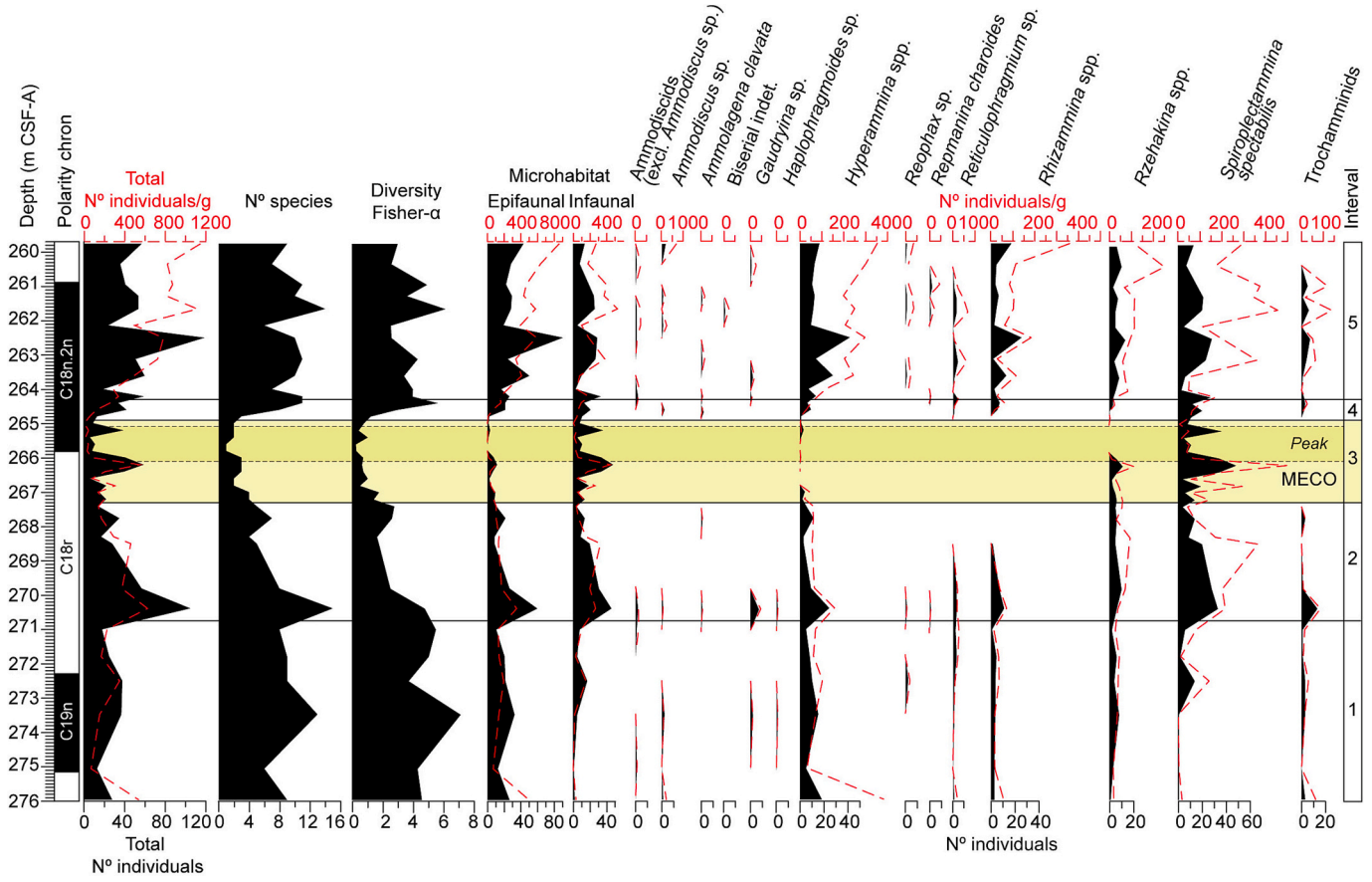

Fig. 3. Agglutinated benthic foraminiferal taxa identified at IODP Site U1511 (Supp. Mat., Table S3), plotted against depth (m CSF-A). Total number of individuals (in black) and total number of individuals per gram of sediment (dashed red lines). Light yellow bar marks the MECO/interval 3; the darker yellow bar marks the MECO peak. (For interpretation of the references to colour in this figure legend, the reader is referred to the web version of this article.)

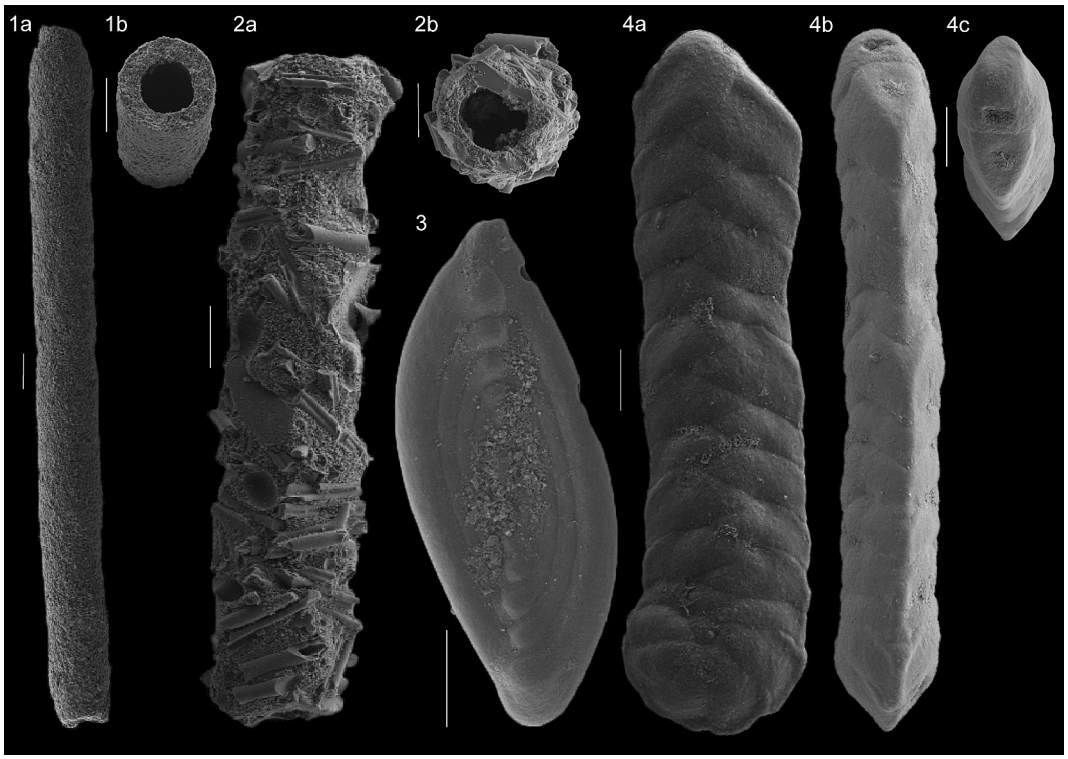

Fig. 4. SEM images of the most common agglutinated benthic foraminiferal taxa across the middle Eocene at IODP Site U1511. 1a-b: *Hyperammina* sp., sample U1511B, 17R (1, 127–129 cm); 2 a-b: *Rhizammina* sp. 2, sample U1511B, 16R (4, 19–21 cm); 3: *Rzehakina* sp., sample U1511B, 17R (3, 136–138 cm); 4 a–c: *Spiroplectammina spectabilis*, sample U1511B, 16R (4, 58–60 cm). All scale bars = 100 μm.

kV, a current of 30 mA, CuKα radiation, automatic slit, and a graphite monochromator. The XRD patterns were acquired from 3 to 60° 2θ for whole sediment samples, and from 3 to 30° 2θ for <2 μm fractions of samples. The goniometer velocity was 0.02° 2θ/s and the integration time was 0.5 s. Analyses were recorded using the XPowder software (Martin, 2017). Relative proportions of mineral phases present in both the whole rock and the <2 μm fraction were determined using Reference Intensity Ratios (RIR) values from Schultz (1964), Biscaye (1965) and Davis and Smith (1988).

4. Results

4.1. Benthic foraminifera

Benthic foraminiferal assemblages at Site U1511 contain only agglutinated taxa. A total of fifteen agglutinated taxa belonging to 9 suborders (Kaminski et al., 2021; Table 1) were identified at the species or higher taxonomic level. These taxa have been allocated to microhabitats (infaunal or epifaunal; Jorissen et al., 1995; Alegret et al., 2003; Table 1), and further classified by their presumed feeding strategy as either suspension-feeding or deposit-feeding (Nagy et al., 1995; Van den Akker et al., 2000; Kaminski and Gradstein, 2005; Table 1).

Based on the distribution and diversity of benthic foraminiferal assemblages, the mineralogical and compositional results, and after combining all these data with previous results from Sutherland et al. (2019) and Cornaggia et al. (2020), the record studied at Site U1511 can be subdivided into five intervals: interval 1 (275.96–270.74 m CSF-A), interval 2 (270.74–267.30 m CSF-A), interval 3 (267.30–264.90 m CSF-A), interval 4 (264.90–264.30 m CSF-A), interval 5 (264.30–259.75 m CSF-A).

The number of individuals is generally low in interval 1, showing a major peak in the lower part of interval 2 (270.38 m CSF-A) and gradually decreasing across this interval and the lower part of interval 3 (Fig. 3). A transient positive peak in the number of individuals and the estimated individuals per gram is observed at the middle part of interval 3 (266.19 m CSF-A). The total number of individuals shows a second major peak in the middle of interval 5, and further decreases towards the top of the study section. The total number of individuals per gram gradually increases towards the top of the study section (Fig. 3). The number of species (between 1 and 15; average 6.71), and the diversity of the assemblages (Fisher-α values between 0.26 and 7.13; average 2.81) are moderate to low throughout the study section, reaching minimum values in interval 3.

The number of epifaunal morphogroups (average of 19.03) is slightly higher than infaunal ones (average of 16.66) across the study section, except for interval 3, which is dominated by infaunal taxa. Infaunal morphogroups include the common to abundant species *Spiroplectammina spectabilis* (Figs. 3 and 4), and rare taxa such as *Reticulophragmium* sp., *Reophax* sp., *Haplophragmoides* sp., *Gaudryina* sp., or some bi-triserial indet (Fig. 3). Among epifaunal morphogroups, *Hyperammina* spp. (Figs. 3 and 4), *Rhizammina* spp. (Figs. 3 and 4), *Rzehakina* spp. (Figs. 3 and 4) and the trochamminids group are the most common taxa; rare taxa include the Ammodiscids group or the species *Ammolagena clavata* (Fig. 3). Benthic foraminiferal assemblages show notable changes in diversity and in the relative abundance of taxa across the study record at Site U1511:

Interval 1 (275.96–270.74 m CSF-A) shows the highest diversity values of the study interval. The epifaunal genus *Hyperammina* dominates the assemblages (Fig. 3); *Rzehakina* and *Rhizammina* are present in this interval. The infaunal *S. spectabilis* becomes common from the middle part of interval 1.

Within interval 2 (270.74–267.30 m CSF-A), assemblages consist of mixed infaunal (e.g., *S. spectabilis*) and epifaunal morphogroups (e.g., *Hyperammina* spp.) (Fig. 3). Diversity of the assemblages gradually decreases across this interval, and several taxa temporarily disappear (ammodiscids, *Ammodiscus* sp., *A. clavata*, *Gaudryina* sp., *Reophax* sp., *R. charoides*, *Reticulophragmium* sp., *Rhizammina* spp., trochamminids). The last occurrence of *Haplophragmoides* sp. has also been recorded in

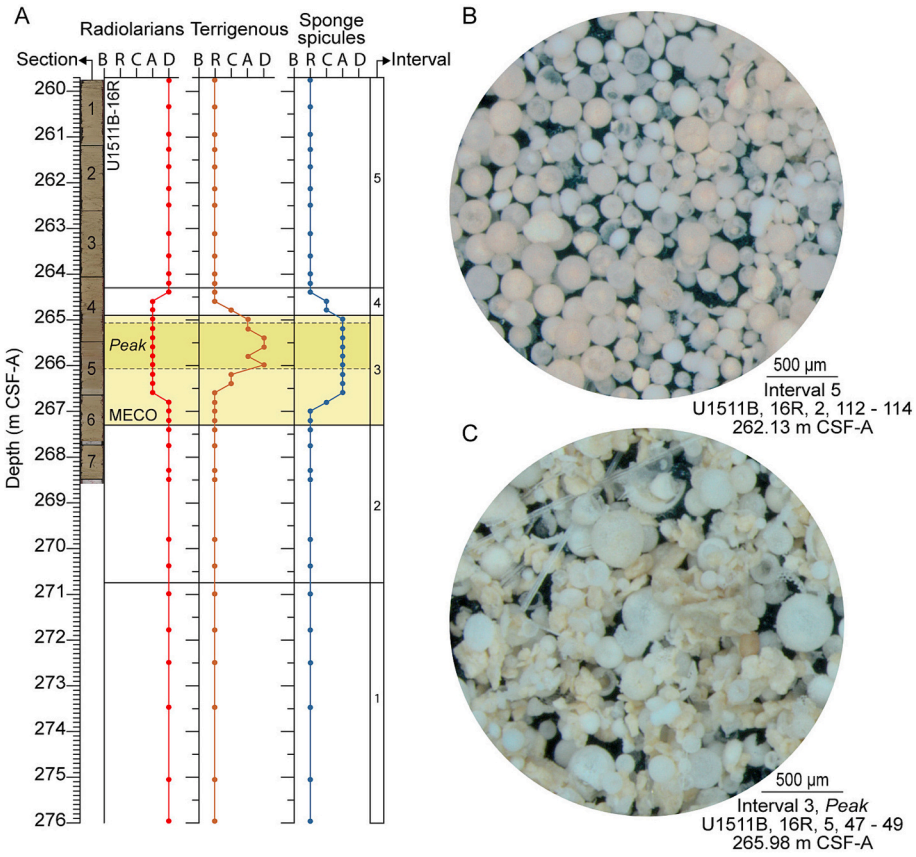

Fig. 5. A) Qualitative assessment of the sediment components (other than benthic foraminifera) at Site U1511 (B = barren, R = rare, C = common, A = abundant, and D = dominant) (Supp. Mat., Table S4). B) Photograph under the reflected light microscope of a sample of the post-MECO interval, showing the clear dominance of radiolarians. C) Photograph under the binocular microscope of a sample of the MECO interval, showing radiolarians as well as sponge spicules and terrigenous material.

Table 1
Agglutinated benthic foraminifera suborders (Kaminski et al., 2021), taxa identified at IODP Site U1511, microhabitats (Jorissen et al., 1995 for all taxa except for *Spiroplectammina spectabilis*, which follows Alegret et al., 2003) and feeding strategy (Nagy et al., 1995; Van den Akker et al., 2000; Kaminski and Gradstein, 2005).

Suborder	Taxa	Microhabitat	Feeding strategy
Astrorhizina	*Rhizammina* sp. 1		
	Rhizammina sp. 2	Epifaunal	Suspension-feeder
Hippocrepinina	*Hyperammina* spp.		Suspension-feeder
	Ammolagena clavata	Epifaunal	Deposit-feeder
Ammodiscina	Ammodiscids		
	Ammodiscus sp.	Epifaunal	Deposit-feeder
	Trochamminids		
	Repmanina charoides		
Schlumbergerinina	*Rzehakina* spp.	Epifaunal	Deposit-feeder
Hormosinina	*Reophax* sp.	Infaunal	Deposit-feeder
Lituolina	*Haplophragmoides* sp.	Infaunal	Deposit-feeder
Spiroplectamminina	*Spiroplectammina spectabilis*	Infaunal	Deposit-feeder
Loftusiina	*Reticulophragmium* sp.	Infaunal	Deposit-feeder
Verneuilinina	*Gaudryina* spp.	Infaunal	Deposit-feeder
	Biserial indet.		

interval 2. *Spiroplectammina spectabilis* becomes the most abundant species (Fig. 3). Other taxa such as *Rhizammina*, *Rzehakina* and the trochamminids group, are also present but in smaller proportions (<20 individuals). The trochamminids group and the genus *Rhizammina* temporally disappear from middle-upper part of this interval, and reappear in interval 4 (Fig. 3).

Interval 3 (267.30–264.90 m CSF-A) shows a marked decline in diversity, with the lowest values of the whole study recorded between 265.86 and 265.57 m CSF-S. Assemblages are dominated by the infaunal *S. spectabilis*, which shows abundance peaks that reach the highest number of specimens per gram (500 individuals/g). The genus *Hyperammina* is very scarce in this interval, showing the lowest values (<5 individuals per sample) (Fig. 3). A minor peak in the abundance of *Rzehakina* in the middle part of interval 3 (266.24 m CSF-A) is followed by the temporary disappearance of this genus.

In interval 4 (264.90–264.30 m CSF-A), diversity of the assemblages rapidly returns to values similar to those observed in interval 1, in contrast to the slow and gradual decline of interval 2 (Fig. 3). *Spiroplectammina spectabilis* remains the dominant taxon, and taxa that temporally disappeared in interval 2 (*Rhizammina* spp., trochamminids, *Reticulophragmium* sp., *R. charoides*, *Gaudryina* sp., *A. clavata*, *Ammodiscus* sp., Ammodiscids) or in interval 3 (*Rzehakina* spp.), reappear (Fig. 3).

Interval 5 (264.30–259.75 m CSF-A) is characterised by a higher number of individuals and individuals/g. The number of *Hyperammina* and *Rhizammina* per gram increases gradually across this interval, showing maximum values in its uppermost sample, at 259.75 m CSF-A. *Spiroplectammina spectabilis* is abundant (maximum of 412.37 individuals/g at 261.65 m CSF-A), and the genus *Rzehakina* and the trochamminids group show their maximum values of individuals/g (227,79 individuals/g at 260,34 m CSF-A and 123.71 individuals/g at 261,65 m CSF-A, respectively) (Fig. 3).

4.2. Other coarse fraction sediment components

Qualitative analysis of sediment composition also reveals significant changes across the study interval. Radiolarians, the primary component of the samples, are abundant across interval 3 and in the lower part of interval 4, but dominant in the other intervals (Fig. 5A). Sponge spicules are a rare component in intervals 1, 2 and 5. In interval 3, their percentage increases progressively from rare to abundant at ~267 m CSF-A, and decreasing again to common and rare from ~264.9 m CSF-A onwards (Fig. 5A). Terrigenous material is rare throughout most of the study material. However, in interval 3, at ~266.6 m CSF-A its percentage gradually increases from rare to abundant and dominant (Fig. 5A), subsequently decreasing back to common and rare in the lower part of interval 4.

The images of Fig. 5B-C illustrate the different sediment composition in intervals 3 and 5.

4.3. Mineralogical composition of the samples

X-ray diffraction analyses indicate that the samples are composed of clay minerals (73–86%), quartz (10–14%) and halite (<5–13%) (see details in the Suppl. Mat., Table S5; Fig. 6). Among the clay minerals, kaolinite, smectite and illite were identified in the <2 μm fractions.

No significant variations in quartz content were observed. The halite content gradually decreases from intervals 1 and 3 (10% and 11%, respectively) to interval 3. Values range between 4% and 11% (average of 7%) in the lower part of interval 3, and the average content is less than 5% in the upper part of this interval (Suppl. Mat., Table S5). The halite content increases in intervals 4 and 5 (6% and 8%, respectively), and clay minerals follow the opposite trend, with higher values in interval 3 (75%–86%, Fig. 6A) than in the rest of the study intervals (73%–83%).

Regarding the composition of the clay minerals, a slight decrease is recorded in the illite and kaolinite content in interval 3 (Fig. 6B), where their average content is 34% and 19%, respectively. This contrasts with their higher percentage in the rest of the study section.

A remarkable increase in the smectite content is recorded in interval 3. Its value ranges from 18% to 13% in intervals 1 and 2, and it doubles within interval 3, ranging from 10% to 41%, with an average of 29%. Subsequently, the smectite content decreases in interval 4 and 5, with values similar to those recorded in intervals 1–2 (Fig. 6B).

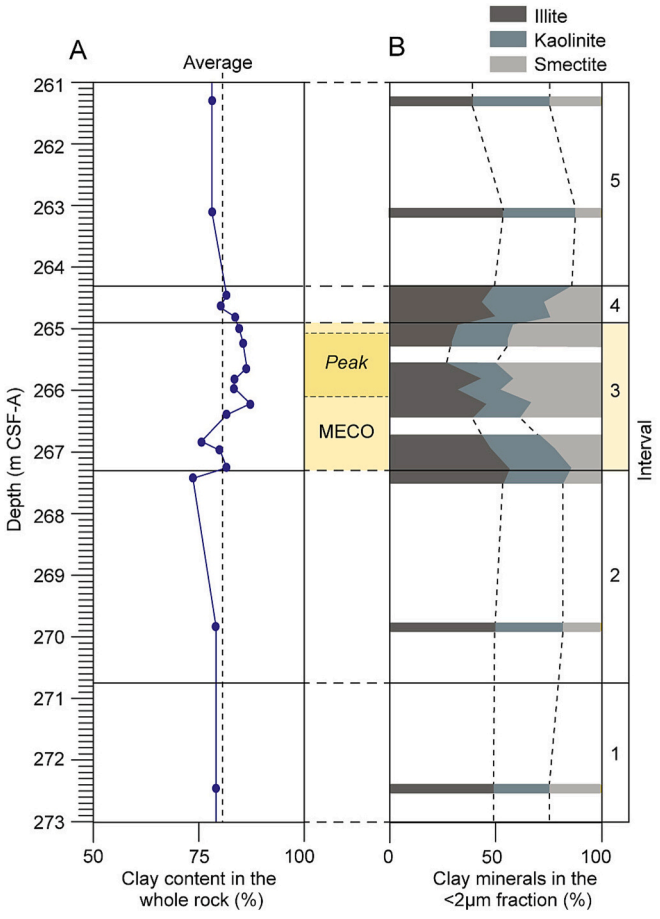

Fig. 6. A. Average clay minerals content, in whole rock; B. Clay mineral assemblages in the <2 μm fraction (Supp. Mat., Table S5).

5. Palaeoenvironmental interpretation across the MECO at IODP Site U1511

According to the refined age model of this study, based on magnetostratigraphic and radiolarian tie points, the MECO at Site U1511 spans from 40.03 to 39.82 Ma (interval 3, 267.30–264.90 m CSF-A), lasting ~202 kyr. This time span is less than other estimates of the duration of the MECO, which range from ~300 kyr (Rivero-Cuesta et al., 2019) to ~500 kyr (Westerhold and Röhl, 2013) or ~650 kyr (e.g., Bohaty et al., 2009; Edgar et al., 2010). The shorter duration of the MECO at Site U1511 may be related to the identification of its lower and upper boundaries, which have been approximated through palaeomagnetic data, the mineralogical composition of the sediment, and the benthic foraminiferal changes. The lack of carbonate sediment and calcareous microfossils at this abyssal site deposited below the CCD prevented the identification of the MECO through traditional $\delta^{18}O$ analyses (Bohaty and Zachos, 2003; Bohaty et al., 2009; Moebius et al., 2015). In addition to new palaeomagnetic data, the refined age model in this site includes radiolarian bioevents from shipboard data, which were obtained at a low sampling resolution for the whole middle Eocene, and not specifically for the MECO. This might also account for the shorter duration of the MECO in this study.

The subinterval between 266.10 and 265.09 m CSF-A shows the greatest environmental perturbation, the lowest diversity of benthic foraminiferal assemblages, the highest terrigenous and smectite content, and it closely aligns with the base of polarity Chron C18n.2n (Figs. 3 and 5). Based on these results, this subinterval has been assigned to the MECO peak warming.

The absence of coarse lithic components at Site U1511 is consistent with an offshore location far from land. The fact that benthic assemblages are represented by DWAF, especially the genus *Hyperammina*, a suspension-feeder genus that inhabits tranquil bathyal and abyssal environments with low organic matter flux (Nagy et al., 1995; Van den Akker et al., 2000; Kaminski and Gradstein, 2005), supports the general oligotrophic conditions at this site. Abyssal plains, like the Tasman Abyssal Plain where Site U1511 was drilled, are environments with low sedimentation and low organic flux, and their DWAF assemblages represent the most oligotrophic end of the spectrum (Kaminski and Gradstein, 2005). The diversity of the assemblages is low across the whole study section (average Fisher-α index = 2.8). The lowest values are recorded across the MECO (average Fisher-α index = 0.8). The highest values (average of 5.1) are recorded below the MECO, and they are close to those recorded at the same site during the early Eocene, when this site already lied below the CCD (average Fisher-α index = 6.0 in cores 36R to 33R; Kaminski et al., 2024a; Suppl. Mat., Table S6). The gradual decline in diversity of the benthic assemblages from interval 2 to the MECO interval reflects gradually increasing environmental stress, which culminated during the peak of the MECO (Figs. 3 and 7). The gradual decrease in diversity and the temporary disappearance of nine taxa (including ammodiscids, *Ammodiscus* sp., *A. clavata, Gaudryina* sp., *Reophax* sp., *R. charoides, Reticulophragmium* sp., *Rhizammina* spp., trochamminids) indicates that environmental stress at the seafloor started in interval 2, which might correspond to the onset of the MECO. These taxa disappear from the fossil record in interval 2 and reappear in

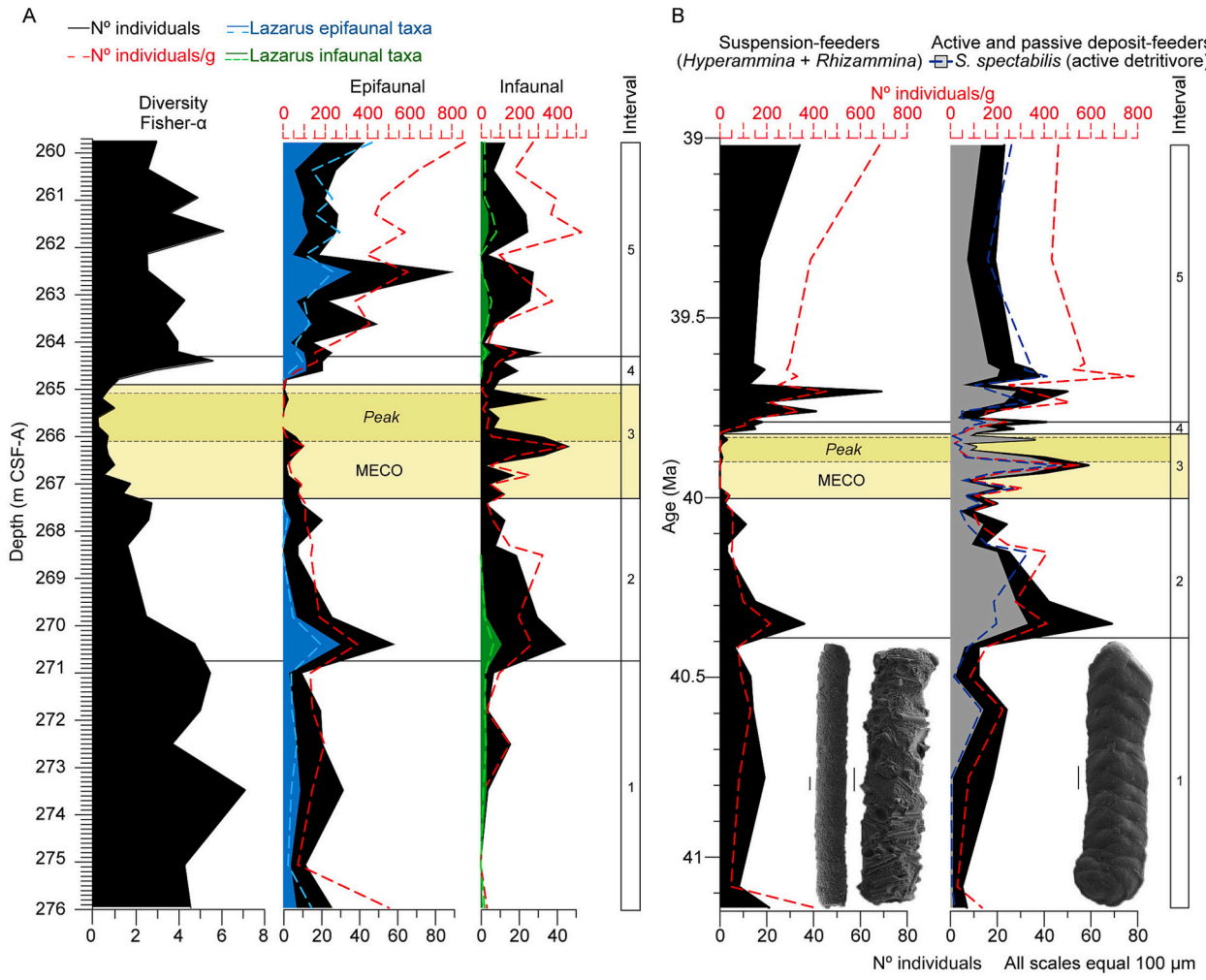

Fig. 7. A. Diversity of benthic foraminiferal assemblages, morphogroups, and Lazarus taxa at IODP Site U1511 (Supp. Mat., Table S3). Epifaunal individuals (in black); epifaunal individuals/g (red dashed line); epifaunal Lazarus individuals (in blue) and epifaunal Lazarus individuals/g (blue dashed lines); infaunal individuals (in black); infaunal individuals/g (red dashed lines); infaunal Lazarus individuals (in green) and infaunal Lazarus individuals/g (green dashed lines) plotted against depth (m CSF-A). B. Total number of individuals (in black) and total number of individuals/g (red dashed lines) of agglutinated benthic foraminifera identified at IODP Site U1511 (Supp. Mat., Table S3), classified according to their feeding strategies (Table 1), plotted against age (Ma). Note that the application of a high overall background sedimentation rate may lead to an underestimation of the duration of the MECO at this site. (For interpretation of the references to colour in this figure legend, the reader is referred to the web version of this article.)

interval 4, and are considered as Lazarus taxa, i.e., taxa that locally disappear from the local stratigraphic record, migrate and survive in refugia ('Lazarus effect'), and later reappear when conditions are more favourable (e. g., Jablonski, 1986). The decline in diversity was primarily driven by a reduction in epifaunal genera such as *Hyperammina*, *Rhizammina*, *Rzehakina* and trochamminids (Fig. 3). This biotic turnover appears to be linked to decreased availability and quality of food (organic carbon) reaching the seafloor during the MECO at Site U1511. The genera *Hyperammina* and *Rhizammina* are tubular suspension-feeding epifaunal forms that attach to substrates and extend pseudopodial networks into the water column to capture food particles (Kaminski and Gradstein, 2005). These taxa, common in lower bathyal to abyssal zones (Schröder, 1986), thrive in areas with gentle boundary currents that deliver suspended food (Kaminski and Gradstein, 2005). Increased water-column stratification during the MECO may have slowed down deep-water currents that brought organic particles to these sessile taxa, leading to their decline during the MECO (Fig. 7). It is unlikely that the decline in tubular suspension feeders was related to decreased oxygenation of bottom waters, as the genus *Hyperammina* and other tubular forms have been reported to survive under poorly oxygenated conditions (Tyszka and Kaminski, 1995). The proliferation of the active-deposit feeder *S. spectabilis* during the MECO (Fig. 7) can be attributed to its opportunistic feeding strategy (Alegret et al., 2022). As a shallow infaunal, active motile detritivore, it feeds on bacteria and detritus from the flocculent layer, using reticulopodia for locomotion and to collect the scarce detritus from sediments (Nagy, 1992; Kaminski and Gradstein, 2005; Mackensen et al., 1995; Arreguín-Rodríguez et al., 2016). The dominance of *S. spectabilis* during the MECO may have been related to its ability to exploit limited and low-quality resources. Additionally, we speculate that warming may have increased remineralization of the organic matter in the water column, reducing food availability at this site during the MECO, but further independent evidence for food availability at the seafloor is needed to test this hypothesis. In contrast to the gradual decline in diversity of the assemblages from intervals 2 to 3, its rapid recovery in interval 4, and the reappearance of most Lazarus taxa that had temporally disappeared in interval 2 (except for the genus *Reophax* and the species *R. charoides*, which reappeared in interval 5; Figs. 3 and 7) (e.g., Thomas, 1990; Alegret et al., 2021b), indicates that environmental conditions at the seafloor rapidly recovered during the post-MECO transition (interval 4). Most of the taxa affected by the Lazarus effect were epifaunal, with the suspension-feeder *Rhizammina* being the most affected one (Fig. 7). This

further supports the idea that warming during the MECO, and subsequent water-column stratification, affected the availability and quality of food reaching the deep-sea, highlighting the importance of the different feeding-strategies. The recovery in the abundance of suspension-feeders in interval 5 (Fig. 7) points to reduced stratification of the water column after the MECO and intensification of bottom-water currents in the Tasman Sea. In the modern Tasman Abyssal Plain, the East Australian Current and its warm core rings have a significant impact on abyssal depths (Mulhearn, 1983), and strong abyssal currents (with fluctuations between 10 and 35 cm s^{-1}) have been measured (Mulhearn et al., 1986). Additionally, the depth to which the East Australian Current and the Tasman Front extend is highly variable (2500 m - 4500 m; Mulhearn et al., 1989). The mechanism through which MECO warming slowed down bottom currents near Site U1511 in the Tasman Abyssal Plain remains to be further investigated, but water column stratification during the MECO may have contributed to weaker near-bottom currents.

The higher-resolution mineralogical analysis here presented supports the results from Cornaggia et al. (2020), revealing a higher content in clay minerals (particularly in smectite) during the MECO at Site U1511 (Fig. 6). Kaolinite and smectite are commonly formed during chemical weathering processes by the dissolution of previous phyllosilicates (such as illite) (Chamley, 1989; Velde, 1995). Chemical weathering processes occur under tropical to subtropical conditions, and the presence of kaolinite and smectite is commonly related to tropical warm and humid climatic conditions (e.g., Singh and Gilkes, 1991; Ehrmann et al., 2005; Raucskik and Varga, 2008; Do Campo et al., 2018; Bauluz et al., 2014; Laita et al., 2024). The higher presence of smectite at Site U1511 during the MECO suggests a tropical to subtropical climate in the source area. It may also indicate sediment provenance during the MECO from a warmer area as a result of a change in ocean currents. The detrital quartz content does not increase during the MECO, and the normalised smectite/quart content increases, indicating there was a real increase in smectite (Suppl. Mat., Table S5). These results preclude the interpretation of the increase in smectite during the MECO as a result on enhanced physical erosion of previously formed clays.

Changes in sediment composition (increase in smectite clay), increased water column stratification and reduced biosiliceous plankton productivity previously reported across the MECO at Site U1511 (Sutherland et al., 2019; Cornaggia et al., 2020) are consistent with the results of this study. The latter study also suggests changes in deep-water masses and lower sedimentation rates during the MECO.

The findings of this study contribute to the growing dataset of the MECO in the Tasman Sea, which may enhance the understanding of how Eocene warming periods impacted surface and deep-sea environments in this area of the Pacific Ocean. Cramwinckel et al. (2020) documented regional southeast Australian transgression and elevated sea-surface temperatures in the Tasmanian gateway during this period, with pollen assemblages pointing to warm temperate rainforests with paratropical elements along Australia's southeastern margin. Data from ODP Site 1172 (Bijl et al., 2010), and from different sites in the Southern Ocean (Bijl et al., 2011) and in the Tasmanian gateway area (ODP Sites 1170 and 1172, Otway Basin and Hampden Beach Section; Cramwinckel et al., 2020) suggest a shift in surface-ocean current configuration coinciding with the peak MECO warmth, but there is not enough data available to support a specific scenario (Cramwinckel et al., 2020). Changes in surface ocean circulation may have influenced bottom currents, as recorded in the modern Tasman Abyssal Plain (Mulhearn, 1983; Mulhearn et al., 1989). Deep water masses were likely forming in the southwest Pacific and Southern Ocean at this time (e.g., Zhang et al., 2022; Peñalver-Clavel et al., 2025). The decreased numbers of suspension-feeders among benthic foraminifera across the MECO (Fig. 7) suggest less vigorous bottom currents near Site U1511 in the Tasman Sea, and enhanced clay mineral (smectite) deposition may also support changes in deep-water source. In turn, the increase in the opportunistic, deposit-feeder *S. spectabilis*, is related to its ability to exploit low-quality resources. Increased remineralization of organic matter in the water column contributed to more oligotrophic conditions for the benthos during other Eocene warming events (Alegret et al., 2021a; Peñalver-Clavel et al., 2024), and it is consistent with the reduced flux of other biogenic components (radiolarians) across the MECO; however, further independent evidence for food availability at the seafloor is needed at abyssal Site U1511.

6. Global ocean productivity across the MECO

Increased ocean surface and export productivity have been documented across the MECO at sites from different latitudes and proximity to the continents in the Southern Ocean, the Tethys, and the Atlantic Ocean (Moebius et al., 2015). Analyses of organic carbon, planktic foraminifera and siliceous microfossils indicate elevated surface productivity during the MECO in the Tethys (Alano section; Luciani et al., 2010; Spofforth et al., 2010), South Atlantic Ocean (ODP Site 1260A; Renaudie et al., 2010), North Atlantic Ocean (ODP Site 1051; Witkowski et al., 2014), and Southern Ocean (ODP Sites 748 and 749; Witkowski et al., 2012). Rather than regional changes in upwelling, Moebius et al. (2015) argued that strengthening of the hydrological cycle during the MECO, and the resulting enhanced runoff from land, was the most plausible mechanism to account for increased eutrophication and surface productivity in many ocean basins. In contrast, $\Delta\delta^{13}C$ data from subtropical ODP Site 1051 (NW Atlantic) suggest a possible decline in export productivity (Bohaty et al., 2009).

The palaeoecological analysis of benthic foraminifera across the MECO at Site U1511 provides an opportunity to assess export productivity and to compare results from the Tasman Sea with global data. The comparison of studies on the impact of the MECO on benthic foraminifera (Fig. 1) reveal both similarities and regional variability in their response to palaeoenvironmental changes associated with the MECO. In the North Atlantic ODP Site 1051 (Moebius et al., 2015), minor changes in benthic foraminifera suggest gradual environmental shifts and sustained export productivity despite warming. In contrast, the South Atlantic ODP Sites 1263 (Boscolo-Galazzo et al., 2014, 2015) and 702 (Rivero-Cuesta et al., 2019) show elevated export productivity during early MECO, followed by decline, with evidence of poleward species shifts. In the Southern Ocean (ODP Site 738; Moebius et al., 2014), shifts in benthic foraminifera occurred despite stable diversity. Elevated surface and export productivity and oxygen depleted waters during the MECO were likely associated with increased continental runoff, triggered by an enhanced hydrological cycle and/or the influence of nutrient-rich surface waters, and by a potential change in bottom water masses of North Pacific origin (Moebius et al., 2014). In the Pacific Ocean, there is only a low-resolution study across the middle Eocene at Allison Guyot seamount (ODP Site 865; Arreguín-Rodríguez et al., 2016), but the interval of the MECO was not sampled. Drawing broader conclusions in the Pacific Ocean is thus not possible due to the lack of studies on benthic foraminifera across the MECO. Studies of shallower Tethyan settings reveal regional variability during the MECO, with hypoxia and organic-rich layers at the Alano section (Boscolo-Galazzo et al., 2013) and minor nutrient changes and no deoxygenation at Capo Mortola (Gandolfi et al., 2024).

These studies reveal the complex and regionally diverse nature of benthic foraminiferal response to the MECO. Its impact on marine productivity was regionally variable, influenced by factors such as depth, nutrient delivery, hydrodynamic conditions, and the specific characteristics of each oceanographic setting. Notably, records from sites located at similar latitudes in different basins, such as Site U1511 (southwest Pacific), Site 702 (Atlantic Ocean; Rivero-Cuesta et al., 2019), and Site 738 (Southern Ocean; Moebius et al., 2014), exhibit distinct responses in benthic foraminiferal assemblages, emphasizing the critical role of ocean circulation during Eocene warm intervals. Both Southern Ocean Site 738 and nearby, southwest Pacific Site U1511, record increased water column stratification during the MECO. Increased export productivity has been documented at Site 738, while a

change in feeding strategies of benthic foraminifera is here reported for abyssal Site U1511, and there is currently no independent evidence to account for a net increase or decrease in export productivity at this abyssal site. Differences in ocean circulation at these high-latitude sites may have modulated the response to the MECO warming. During the Eocene, shallower Site 738 was located in the Indian sector of the Southern Ocean (Fig. 1), which might have been influenced by a change in bottom water masses of North Pacific origin during the peak MECO warming (Moebius et al., 2014). In contrast, southwest Pacific Site U1511 was located within an oligotrophic setting in the Tasman Abyssal Plain (Fig. 1), a tectonically active area during the Eocene (Sutherland et al., 2020). Tectonic activity likely altered oceanic circulation and heat transport in the Tasman Sea (e.g., Baatsen et al., 2020; Peñalver-Clavel et al., 2025), which could have significantly shaped the observed MECO effects at Site U1511.

7. Conclusions

Middle Eocene foraminiferal assemblages at IODP Site U1511 consist of deep-water agglutinated foraminifera, which were able to populate the sediments deposited beneath the CCD at this oligotrophic setting in the Tasman Abyssal Plain. The study of deep-water benthic foraminiferal assemblages indicates a gradual onset of the environmental perturbations associated with the MECO, followed by a rapid recovery to pre-MECO conditions. Significant changes in benthic assemblages and in sediment composition indicate that increased stratification of the water column during MECO warming altered both surface and deep-sea ecosystems in the Tasman Sea. The decrease in suspension-feeders points to weaker bottom-water currents, and the temporary disappearance of nine Lazarus taxa and the dominance of the opportunistic species *S. spectabilis* support environmental stress and a change in feeding strategies during the MECO, which favoured motile detritivores that were able to feed on bacteria and detritus from the flocculent layer. Changes in the mineralogical composition of the sediment support this palaeoenvironmental interpretation, with an increase in the smectite content indicating warm and humid climatic conditions in the source area; this might also indicate sediment provenance during the MECO from a warmer area as a result of a change in ocean currents. The reappearance of the Lazarus taxa during the post-MECO interval supports the rapid recovery of the environmental conditions in the deep-sea.

The combination of these results with previous studies in the Tasman Sea allow us to highlight the interconnected effects of warming, ocean stratification, and nutrient cycling on marine ecosystems. This study adds to several lines of evidence that indicate highly variable effects of the MECO warming on marine productivity and benthic ecosystems, locally shaped by oceanographic conditions and palaeogeography.

CRediT authorship contribution statement

Irene Peñalver-Clavel: Writing – review & editing, Writing – original draft, Investigation, Formal analysis, Data curation, Conceptualization. **Elisa Laita:** Writing – review & editing, Writing – original draft, Formal analysis, Data curation. **Edoardo Dallanave:** Writing – review & editing, Data curation. **Rupert Sutherland:** Writing – review & editing, Data curation. **Gerald R. Dickens:** Writing – review & editing. **Thomas Westerhold:** Writing – review & editing. **Blanca Bauluz:** Writing – review & editing, Conceptualization. **Laia Alegret:** Writing – review & editing, Supervision, Project administration.

Declaration of competing interest

The authors declare that they have no known competing financial interests or personal relationships that could have appeared to influence the work reported in this paper.

Acknowledgments

This research is supported by projects PID2023-149894OB-I00, PID2021-123127OB-I00 (MCIN/AEI/10.13039/501100011033, FEDER, UE) and E33_23R (Gobierno de Aragón). IP was supported by the Spanish Ministry of Science and Innovation (MCIN) (FPI grant PRE2020-092638). This publication is part of the grant JDC2022-048348-I funded by the MCIN/AEI/10.13039/501100011033 and by the European Union "NextGenerationEU"/PRTR. Additional funding was provided by the Deutsche Forschungsgemeinschaft (DFG, German Research Foundation) under Germany's Excellence Strategy – EXC-2077–390741603 to TW, and by Deutsche Forschungsgemeinschaft Project Number 465492305 to ED. We acknowledge the use of Servicio General de Apoyo a la Investigación-SAI, Universidad de Zaragoza, and Cristina Gallego for SEM imaging. This research used samples and data provided by the International Ocean Discovery Program (IODP).

Appendix A. Supplementary data

Supplementary data to this article can be found online at https://doi.org/10.1016/j.palaeo.2026.113590.

Data availability

Data generated in this study are available in the Supplementary and at Zenodo, https://doi.org/10.5281/zenodo.18398855 (Peñalver-Clavel et al., 2026).

References

Alegret, L., Thomas, E., 2001. Upper Cretaceous and lower Paleogene benthic foraminifera from northeastern Mexico. Micropaleontology 47 (4), 269–316.
Alegret, L., Molina, E., Thomas, E., 2003. Benthic foraminiferal turnover across the Cretaceous/Paleogene boundary at Agost (southeastern Spain): paleoenvironmental inferences. Mar. Micropaleontol. 48, 251–279.
Alegret, L., Harper, D.T., Agnini, C., Newsham, C., Westerhold, T., Cramwinckel, M.J., Dallanave, E., Dickens, G.R., Sutherland, R., 2021a. Biotic response to early Eocene warming events: integrated record from offshore Zealandia, North Tasman Sea. Paleoceanogr. Paleoclimatol. 36, e2020PA004179. https://doi.org/10.1029/2020PA004179.
Alegret, L., Arreguín-Rodríguez, G.J., Trasviña-Moreno, C.A., Thomas, E., 2021b. Turnover and stability in the deep sea: benthic foraminifera as tracers of Paleogene global change. Global Planet. Change 196, 103372. https://doi.org/10.1016/j.gloplacha.2020.103372.
Alegret, L., Arreguín-Rodríguez, G.J., Thomas, E., 2022. Oceanic productivity after the Cretaceous/Paleogene impact: where do we stand? The view from the deep. In: Koeberl, C., Claeys, P., Montanari, A. (Eds.), From the Guajira Desert to the Apennines, and From Mediterranean Microplates to the Mexican Killer Asteroid: Honoring the Career of Walter Alvarez. Geol. Soc. Am. Special Paper, 557 (21). https://doi.org/10.1130/2022.2557(21).
Arreguín-Rodríguez, G.J., Alegret, L., Ortiz, S., 2013. Glomospira acme during the paleocene-eocene thermal maximum: response to $CaCO_3$ dissolution or to ecological forces? J. Foramin. Res. 43 (1), 40–54.
Arreguín-Rodríguez, G.J., Alegret, L., Thomas, E., 2016. Late Paleocene – middle Eocene benthic foraminifera on a Pacific seamount (Allison Guyot, ODP Site 865): greenhouse climate and superimposed hyperthermal events: benthic foraminifera on a Pacific seamount. Paleoceanography 31 (3), 346–364. https://doi.org/10.1002/2015PA002837.
Baatsen, M., Von der Heydt, A.S., Huber, M., Kliphuis, M.A., Bijl, P.K., Sluijs, A., Dijkstra, H.A., 2020. The Middle-to-Late Eocene Greenhouse Climate, Modelled Using the CESM 1.0.5. CPD. https://doi.org/10.5194/cp-2020-29.
Bauluz, B., Yuste, A., Mayayo, M.J., Canudo, J.I., 2014. Early kaolinization of detrital Weald facies in the Galve Subbasin (Central Iberian Chain, north-east Spain) and its relationship to paleoclimate. Cretac. Res. 50, 214–227. https://doi.org/10.1016/j.cretres.2014.03.014.
Bijl, P.K., Houben, A.J.P., Schouten, S., Bohaty, S.M., Sluijs, A., Reichart, G.-J., Damsté, J.S.S., Brinkhuis, H., 2010. Transient middle Eocene atmospheric CO2 and temperature variations. Science 330, 819–821. https://doi.org/10.1126/science.1193654.
Bijl, P.K., Pross, J., Warnaar, J., Stickley, C.E., Huber, M., Guerstein, R., Houben, A.J.P., Sluijs, A., Visscher, H., Brinkhuis, H., 2011. Environmental Forcings of Paleogene Southern Ocean Dinoflagellate Biogeography. Department of Earth, Atmospheric, and Planetary Sciences Faculty Publications (Paper 174, docs.lib.purdue.edu/easpubs/174).
Bijl, P.K., Bendle, J.A.P., Bohaty, S.M., Pross, J., Schouten, S., Tauxe, L., Stickley, C.E., Mckay, R.M., Röhl, U., Olney, M., et al., 2013. Eocene cooling linked to early flow

across the Tasmanian Gateway. Proc. Natl. Acad. Sci. U.S.A. 110, 9645–9650. https://doi.org/10.1073/pnas.1220872110.
Biscaye, P.E., 1965. Mineralogy and sedimentation of recent deep-sea clay in the Atlantic Ocean and adjacent seas and oceans. Geol. Soc. Am. Bull. 76, 803–832. https://doi.org/10.1130/00167606(1965)76[803:MASORD]2.0.CO;2.
Bohaty, S.M., Zachos, J.C., 2003. Significant Southern Ocean warming event in the late middle Eocene. Geology 31, 1017–1020. https://doi.org/10.1130/G19800.1.
Bohaty, S.M., Zachos, J.C., Florindo, F., Delaney, M.L., 2009. Coupled greenhouse warming and deep-sea acidification in the middle Eocene. Paleoceanography 24, PA2207. https://doi.org/10.1029/2008PA001676.
Boscolo-Galazzo, F., Giusberti, L., Luciani, V., Thomas, E., 2013. Paleoenvironmental changes during the Middle Eocene Climatic Optimum (MECO) and its aftermath: the benthic foraminiferal record from the Alano section (NE Italy). Palaeogeogr. Palaeoclimatol. Palaeoecol. 378, 22–35.
Boscolo-galazzo, F., Thomas, E., Pagani, M., Warren, C., Luciani, V., Giusberti, L., 2014. The middle Eocene climatic optimum (MECO): a multiproxy record of paleoceanographic changes in the southeast Atlantic (ODP Site 1263, Walvis Ridge). Paleoceanography 29, 2014PA002670. https://doi.org/10.1002/2014PA002670.
Boscolo-Galazzo, F., Thomas, E., Giusberti, L., 2015. Benthic foraminiferal response to the Middle Eocene Climatic Optimum (MECO) in the South-Eastern Atlantic (ODP Site 1263). Palaeogeogr. Palaeoclimatol. Palaeoecol. 417, 432–444. https://doi.org/10.1016/j.palaeo.2014.10.004.
Cande, S.C., Stock, J.M., 2004. Cenozoic reconstructions of the Australia-New Zealand-South Pacific Sector of Antarctica. In: Exon, N.F., Kennett, J.P., Malone, M.J. (Eds.), The Cenozoic Southern Ocean: Tectonics, Sedimentation, and Climate Change Between Australia and Antarctica. AGU, Washington, DC, pp. 5–17 available at: http://resolver.caltech.edu/CaltechAUTHORS:20140425-125510082.
Cao, W., Zahirovic, S., Flament, N., Williams, S., Golonka, J., Dietmar Müller, R., 2017. Improving global paleogeography since the late Paleozoic using paleobiology. Biogeosciences 14 (23), 5425–5439. https://doi.org/10.5194/bg-14-5425-2017.
Chamley, H., 1989. Clay Sedimentology. Springer-Verlag, Berlin, Heidelberg New York, p. 623.
Cornaggia, F., Bernardini, S., Giorgioni, M., Silva, G.L.X., Nagy, A.I.M., Jovane, L., 2020. Abyssal oceanic circulation and acidification during the Middle Eocene Climatic Optimum (MECO). Sci. Rep. 10 (1), 6674. https://doi.org/10.1038/s41598-020-63525-3.
Cramwinckel, M.J., Huber, M., Kocken, I.J., Agnini, C., Bijl, P.K., Bohaty, S.M., Frieling, J., Goldner, A., Hilgen, F.J., Kip, E.L., et al., 2018. Synchronous tropical and polar temperature evolution in the Eocene. Nature 559, 382–386. https://doi.org/10.1038/s41586-018-0272-2.
Cramwinckel, M.J., Van der Ploeg, R., Bijl, P.K., Peterse, F., Bohaty, S.M., Röhl, U., Schouten, S., Middelburg, J.J., Sluijs, A., 2019. Harmful algae and export production collapse in the equatorial Atlantic during the zenith of Middle Eocene Climatic Optimum warmth. Geology 47, 247–250. https://doi.org/10.1130/G45614.1.
Cramwinckel, M.J., Woelders, L., Huurdeman, E.P., Peterse, F., Gallagher, S.J., Pross, J., Burgess, C.E., Reichart, G.J., Sluijs, A., Bijl, P.K., 2020. Surface-circulation change in the Southwest Pacific Ocean across the middle eocene climatic optimum: inferences from dinoflagellate cysts and biomarker paleothermometry. CP 16, 1667–1689. https://doi.org/10.5194/cp-16-1667-2020.
Dallanave, E., 2024. Assessing the reliability of paleomagnetic datasets using the R package PmagDiR. Sci. Rep. 14 (1666). https://doi.org/10.1038/s41598-024-52001-x.
Dallanave, E., Chang, L., 2020. Early Eocene to Early Miocene magnetostratigraphic framework for IODP Expedition 371 (Tasman Frontier subduction initiation and Paleogene climate). Newsl. Stratigr. 53, 365–387. https://doi.org/10.1127/nos/2019/0556.
Davis, B., Smith, D.K., 1988. Tables of experimental reference intensity ratios. Powder Diffract. 3 (4), 205–208. https://doi.org/10.1017/S088571560001349X.
Do Campo, M., Bauluz, B., Del Papa, C., White, T., Yuste, A., Mayayo, M.J., 2018. Evidence of cyclic climatic changes recorded in clay mineral assemblages from a continental Paleocene-Eocene sequence, northwestern Argentina. Sediment. Geol. 368, 44–57. https://doi.org/10.1016/j.sedgeo.2018.03.007.
Edgar, K.M., Wilson, P.A., Sexton, P.F., Gibbs, S.J., Roberts, A.P., Norris, R.D., 2010. New biostratigraphic, magnetostratigraphic and isotopic insights into the Middle Eocene Climatic Optimum in low latitudes. Palaeogeogr. Palaeoclimatol. Palaeoecol. 297, 670–682. https://doi.org/10.1016/j.palaeo.2010.09.016.
Ehrmann, W., Setti, M., Marinoni, L., 2005. Clay minerals in Cenozoic sediments off Cape Roberts (McMurdo Sound, Antarctica) reveal palaeoclimatic history. Palaeogeogr. Palaeoclimatol. Palaeoecol. 229, 187–211. https://doi.org/10.1016/j.palaeo.2005.06.022.
Gandolfi, A., Giraldo-Gómez, V.M., Luciani, V., Piazza, M., Brombin, V., Crobu, S., Papazzoni, C.A., Pignatti, J., Briguglio, A., 2024. Unraveling ecological signals related to the MECO onset through planktic and benthic foraminiferal records along a mixed carbonate-siliciclastic shallow-water succession. Mar. Micropaleontol. 190 (2024), 102388. ISSN 0377-8398. https://doi.org/10.1016/j.marmicro.2024.102388.
Gradstein, F.M., Ogg, J.G., Schmitz, M.D., Ogg, G.M. (Eds.), 2020. Geological Time Scale. Elsevier. https://doi.org/10.1016/B978-0-12-824360-2.00001-2.
Henehan, M.J., Edgar, K.M., Foster, G.L., Penman, D.E., Hull, P.M., Greenop, R., Anagnostou, E., Pearson, P.N., 2020. Revisiting the Middle Eocene Climatic Optimum "Carbon Cycle Conundrum" with new estimates of atmospheric pCO2 from boron isotopes. Paleoceanogr. Paleoclimatol. 35, e2019PA003713. https://doi.org/10.1029/2019PA003713.
Huber, M., Brinkhuis, H., Stickley, C.E., Döos, K., Sluijs, A., Warnaar, J., Schellenberg, S.A., Williams, G.L., 2004. Eocene circulation of the Southern Ocean: was Antarctica kept warm by subtropical waters? Paleoceanography 19 (4). https://doi.org/10.1029/2004pa001014.
Huck, C.E., Van de Flierdt, T., Bohaty, S.M., Hammond, S.J., 2017. Antarctic climate, Southern Ocean circulation patterns, and deep-water formation during the Eocene. Paleoceanography 32, 674–691. https://doi.org/10.1002/2017PA003135.
Jablonski, D., 1986. Background and mass extinctions: the alternation of macroevolutionary regimes. Science 231 (4734), 129–133.
Jorissen, F.J., Stigter, H.C., Widmark, J.G.V., 1995. A conceptual model explaining benthic foraminiferal microhabitats. Mar. Micropaleontol. 26, 3–15.
Kaminski, M.A., Gradstein, F.M., 2005. Cenozoic Cosmopolitan Deep-water Agglutinated Foraminifera, 10. Grzybowski Foundation Special Publications, p. 547.
Kaminski, M.A., Alegret, L., Hikmahtiar, S., Waśkowska, A., 2021. The Paleocene of IODP Site U1511, Tasman Sea: a lagerstätte deposit for deep-water agglutinated foraminifera. Micropaleontology 67 (4), 341–364. https://doi.org/10.47894/mpal.67.4.02.
Kaminski, M.A., Alegret, L., Hikmahtiar, S., Waśkowska, A., 2024a. The Paleocene of IODP Site U1511, Tasman Sea: a lagerstätte deposit for deep-water agglutinated foraminifera: part 2. Micropaleontology 70 (3), 271–285 plates 1–2, text-figures 1–3, table 1. 10.47894/mpal.70.3.06.
Kaminski, M.A., Korin, A., Hikmahtiar, S., Alegret, L., Waskowska, A., 2024b. The global extent of Paleocene to Eocene deep-water agglutinated foraminiferal acmes. Stratigraphy 21 (4), 279–286.
Kennett, J.P., 1977. Cenozoic evolution of Antarctic glaciation, circum-Antarctic Ocean, and their impact on global paleoceanography. J. Geophys. Res. 82 (27), 3843–3860. https://doi.org/10.1029/JC082i027p03843.
Laita, E., Abad, I., Reolid, M., 2024. Palaeoclimatic inferences from Clayey-Iron Palaeosols: a weathering event recorded in the Middle-Upper Jurassic unconformity (South Iberian Palaeomargin, Western Tethys). Minerals 14 (8), 741. https://doi.org/10.3390/min14080741.
Luciani, V., Giusberti, L., Agnini, C., Fornaciari, E., Rio, D., Spofforth, D.J.A., Pälike, H., 2010. Ecological and evolutionary response of Tethyan planktonic foraminifera to the Middle Eocene Climatic Optimum (MECO) from the Alano section (NE Italy). Palaeogeogr. Palaeoclimatol. Palaeoecol. 292 (1–2), 82–95.
Lyle, M., Lyle, A.O., Backman, J., Tripati, A., 2005. Biogenic sedimentation in the Eocene equatorial Pacific – the stuttering greenhouse and Eocene carbonate compensation depth. In: Proceedings of the Ocean Drilling Program: Scientific Results, ODP Leg, 199, pp. 1–35.
Mackensen, A., Schmiedl, G., Harloff, J., Giese, M., 1995. Deep-sea foraminifera in the south Atlantic Ocean: ecology and assemblage generation. Micropaleontology 41, 342–358.
Martin, J.D., 2017. A software package for powder X-ray diffraction analysis. In: Qualitative, Quantitative and Microtexture, p. 121. Available online: www.xpowder.com.
Moebius, I., Friedrich, O., Scher, H.D., 2014. Changes in Southern Ocean bottom water environments associated with the Middle Eocene Climatic Optimum (MECO). Palaeogeogr. Palaeoclimatol. Palaeoecol. 405, 16–27. https://doi.org/10.1016/j.palaeo.2014.04.
Moebius, I., Friedrich, O., Edgar, K.M., Sexton, P.F., 2015. Episodes of intensified biological productivity in the subtropical Atlantic Ocean during the termination of the Middle Eocene Climatic Optimum (MECO). Paleoceanography 30, 1041–1058. https://doi.org/10.1002/2014PA002673.
Mulhearn, P.J., 1983. Deep currents of the northern Tasman Sea Basin. Deep Sea Res. A 30 (11), 1119–1126.
Mulhearn, P.J., Filloux, J.H., Lilley, F.E.M., Bindoff, N.L., Ferguson, I.J., 1986. Abyssal currents during the formation and passage of a warm-core ring in the East Australian current. Deep Sea Res. A 33 (11–12), 1563–1576.
Mulhearn, P.J., Hamilton, L., Scott, B., 1989. Deep Structure of the East Australian Current and Tasman Front. WSRL-TM-7/89, AR 005-869.
Müller, R.D., Seton, M., Zahirovic, S., Williams, S.E., Matthews, K.J., Wright, N.M., et al., 2016. Ocean basin evolution and global-scale plate reorganization events since Pangea breakup. Annu. Rev. Earth Planet. Sci. 44, 107–138. https://doi.org/10.1146/annurev-earth-060115-012211.
Müller, R.D., Cannon, J., Qin, X., Watson, R.J., Gurnis, M., Williams, S., Pfaffelmoser, T., Seton, M., Russell, S.H.J., Zahirovic, S., 2018. GPlates: building a virtual earth through deep time. Geochem. Geophys. Geosyst. 19, 2243–2261.
Nagy, J., 1992. Environmental significance of foraminiferal morphogroups in Jurassic North Sea deltas. Palaeogeogr. Palaeoclimatol. Palaeoecol. 95 (1–2), 111–134.
Nagy, J., Gradstein, F.M., Kaminski, M.A., Holbourn, A.E.L., 1995. Late Jurassic to Early Cretaceous foraminifera of Thakkhola, Nepal: palaeoenvironments and description of new taxa. In: Kaminski, M.A., Geroch, S., Gasinski, M.A. (Eds.), Proceedings of the Fourth International Workshop on Agglutinated Foraminifera, 3. Grzybowski Foundation Special Publication, pp. 181–209.
Pälike, H., Lyle, M., Nishi, H., et al., 2012. A Cenozoic record of the equatorial Pacific carbonate compensation depth. Nature 488, 609–614. https://doi.org/10.1038/nature11360.
Peñalver-Clavel, I., Agnini, C., Westerhold, T., Cramwinckel, M.J., Dallanave, E., Bhattacharya, J., Sutherland, R., Alegret, L., 2024. Integrated record of the Late Lutetian thermal maximum at IODP site U1508, Tasman Sea: the deep-sea response. Mar. Micropaleontol. 191, 102390. https://doi.org/10.1016/j.marmicro.2023.102390.
Peñalver-Clavel, I., Batenburg, S.J., Sutherland, R., Dallanave, E., Dickens, G.R., Westerhold, T., Agnini, C., Alegret, L., 2025. Intensified bottom water formation in the southwest Pacific during the early Eocene greenhouse – insights from neodymium isotopes. Geology 2025. https://doi.org/10.1130/G52974.1.
Raucskik, B., Varga, A., 2008. Climato-environmental controls on clay mineralogy of the Hettangian-Bajocian successions of the Mecsek Mountains, Hungary: an evidence for

extreme continental weathering during the early Toarcian oceanic anoxic event. Palaeogeogr. Palaeoclimatol. Palaeoecol. 265, 1–13. https://doi.org/10.1016/j.palaeo.2008.02.004.

Renaudie, J., Danelian, T., Saint, Martin S., Le Callonnec, L., Tribovillard, N., 2010. Siliceous phytoplankton response to a middle Eocene warming event recorded in the tropical Atlantic (Demerara Rise, ODP Site 1260A). Palaeogeogr. Palaeoclimatol. Palaeoecol. 286 (3–4), 121–134.

Rivero-Cuesta, L., Westerhold, T., Agnini, C., Dallanave, E., Wilkens, R.H., Alegret, L., 2019. Paleoenvironmental changes at ODP Site 702 (South Atlantic): anatomy of the Middle Eocene Climatic Optimum. Paleoceanogr. Paleoclimatol. 34. https://doi.org/10.1029/2019PA003806.

Schröder, C.J., 1986. Deep-water arenaceous foraminifera in the northwest Atlantic Ocean. In: Canadian Technical Report of Hydrography and Ocean Sciences, 71, p. 191.

Schultz, L.G., 1964. Quantitative interpretation of mineralogical composition from X-ray and chemical data for the Pierre Shale. US Geol. Surv. Prof. Pap. 391-c, 1–31.

Sijp, W.P., Von der Heydt, A.S., Dijkstra, H.A., Flögel, S., Douglas, P.M.J., Bijl, P.K., 2014. The role of ocean gateways on cooling climate on long time scales. Glob. Planet. Change 119, 1–22. https://doi.org/10.1016/j.gloplacha.2014.04.004.

Singh, B., Gilkes, R.J., 1991. A potassium-rich beidellite from a laterite pallid zone in western Australia. Clay Miner. 26, 233–244. https://doi.org/10.1180/claymin.1991.026.2.07.

Spofforth, D.J.A., Agnini, C., Pälike, H., Rio, D., Fornaciari, E., Giusberti, L., Luciani, V., Lanci, L., Muttoni, G., 2010. Organic carbon burial following the middle Eocene climatic optimum in the central western Tethys. Paleoceanography 25, PA3210. https://doi.org/10.1029/2009PA001738.

Steinthorsdottir, M., Vajda, V., Pole, M., Holdgate, G., 2019. Moderate levels of Eocene pCO2 indicated by Southern Hemisphere fossil plant stomata. Geology 47, 914–918. https://doi.org/10.1130/G46274.1.

Sutherland, R., Collot, J., Bache, F., Henrys, S., Barker, D., Browne, G.H., Lawrence, M.J. F., Morgans, H.E.G., Hollis, C.J., Clowes, C., et al., 2017. Widespread compression associated with Eocene Tonga-Kermadec subduction initiation. Geology 45, 355–358. https://doi.org/10.1130/G38617.1.

Sutherland, R., Dickens, G.R., Blum, P., Agnini, C., Alegret, L., Asatryan, G., et al., 2019. Expedition 371 Methods. - Proceedings International Ocean Discovery Program, 371, pp. 1–65. https://doi.org/10.14379/iodp.proc.371.2019.

Sutherland, R., Dickens, G.R., Blum, P., Agnini, C., Alegret, L., Asatryan, G., Bhattacharya, J., Bordenave, A., Chang, L., Collot, J., et al., 2020. Continental-scale geographic change across Zealandia during Paleogene subduction initiation. Geology 48, 419–424. https://doi.org/10.1130/G47008.1.

Thomas, E., 1990. Late Cretaceous-early Eocene mass extinctions in the deep sea. Geol. Soc. Am. Spec. Publ. 247, 481–495. https://doi.org/10.1130/SPE247-p481.

Totterdell, J.M., Blevin, J.E., Struckmeyer, H.I.M., Bradshaw, B.E., Colwell, J.B., Kennard, J.M., 2000. A new sequence framework for the Great Australian Bight: starting with a clean slate. APPEA J. 40, 95–118. https://doi.org/10.1071/aj99007.

Tyszka, J., Kaminski, M.A., 1995. Factors controlling the distribution of agglutinated foraminifera in Aalenian-Bajocian dysoxic facies (Pieniny Klippen Belt, Poland). In: Kaminski, M.A., Geroch, S., Gasinski, M.A. (Eds.), Proceedings of the Fourth International Workshop on Agglutinated Foraminifera, 3. Grzybowski Foundation Special Publication, pp. 271–291.

Van den Akker, T.J.H.A., Kaminski, M.A., Gradstein, F.M., Wood, J., 2000. Campanian to Palaeocene biostratigraphy and palaeoenvironments in the Foula Sub-basin, west of the Shetland Islands, UK. J. Micropaleontol. 19 (1), 23–43.

Van der Ploeg, R., Selby, D., Cramwinckel, M.J., Li, Y., Bohaty, S.M., Middelburg, J.J., Sluijs, A., 2018. Middle Eocene greenhouse warming facilitated by diminished weathering feedback. Nat. Commun. 9, 2877. https://doi.org/10.1038/s41467-018-05104-9.

Velde, B., 1995. Origin and Mineralogy of Clays. Clays and the Environment. SpringerVerlag, Berlin, Heidelberg New York, p. 334.

Westerhold, T., Marwan, N., Drury, A.J., Liebrand, D., Agnini, C., Anagnostou, E., Barnet, J.S.K., Bohaty, S.M., De Vleeschouwer, D., Florindo, F., Frederichs, T., Hodell, D.A., Holbourn, A.E., Kroon, D., Lauretano, V., Littler, K., Lourens, L.J., Lyle, M., Pälike, H., Röhl, U., Tian, J., Wilkens, R.H., Wilson, P.A., Zachos, 2020. An astronomically dated record of earth's climate and its predictability over the last 66 million years. Science 369, 1383–1387. https://doi.org/10.1126/science.aba6853.

Westerhold, T., Röhl, U., 2013. Orbital pacing of Eocene climate during the Middle eocene climate optimum and the chron C19r event: missing link found in the tropical western Atlantic: orbital pacing of Eocene climate. Geochem. Geophys. Geosyst. 14, 4811–4825.

Westerhold, T., Röhl, U., Frederichs, T., Agnini, C., Raffi, I., Zachos, J.C., Wilkens, R.H., 2017. Astronomical calibration of the Ypresian timescale: implications for seafloor spreading rates and the chaotic behavior of the solar system? CP 13 (9), 1129–1152. https://doi.org/10.5194/cp-13-1129-2017.

Witkowski, J., Bohaty, S.M., Mccartney, K., Harwood, D.M., 2012. Enhanced siliceous plankton productivity in response to middle Eocene warming at Southern Ocean ODP Sites 748 and 749. Palaeogeogr. Palaeoclimatol. Palaeoecol. 326, 78–94.

Witkowski, J., Bohaty, S.M., Edgar, K.M., Harwood, D.M., 2014. Rapid fluctuations in mid-latitude siliceous plankton production during the Middle Eocene Climatic Optimum (ODP Site 1051, western North Atlantic). Mar. Micropaleontol. 106, 110–129.

Zachos, J.C., Dickens, G.R., Zeebe, R.E., 2008. An early Cenozoic perspective on greenhouse warming and carbon-cycle dynamics. Nature 451, 279–283. https://doi.org/10.1038/nature06588.

Zhang, Y., De Boer, A.M., Lunt, D.J., Hutchinson, D.K., Ross, P., Van de Flierdt, T., et al., 2022. Early Eocene Ocean meridional overturning circulation: the roles of atmospheric forcing and strait geometry. Paleoceanogr. Paleoclimatol. 37, e2021PA004329. https://doi.org/10.1029/2021PA004329.